PHYSICAL REVIEW B VOLUME 24, NUMBER 4 15 AUGUST 1981

Effects of quantitative disorder on the electronic structures of Si and Ge

Kazuyoshi Tanaka and Raphael Tsu
Energy Conversion Devices, Inc., Troy, Michigan 48084
(Received 13 April 1981)

We have attempted to model the electronic structures of glow-discharge amorphous-Si-based alloys by studying the effects of *specific* kinds of quantitative disorder on the band structures of crystalline Si. A realistic tight-binding Hamiltonian has been developed, including third-nearest-neighbor interactions, which reasonably describes both the valence and first three conduction bands of the crystalline materials. Quantitative disorder is investigated by transforming a disordered system of identical atoms to an ordered diamondlike system with disordered potentials. We find that, in both Si and Ge, bond-length distortions affect mainly the bottom of the valence band at Γ_1 and the low-density-of-states region around X_1, as well as the peaks of $L_{2'}$ and L_1. One might expect, therefore, that localization would be present in both regions near Γ_1 and X_1. Moreover, bond-length distortions affect the bottom of the conduction-band edge in Ge but not in Si. Bond-angle distortions are found to cause shifts of band, primarily in the p-like regions of valence band. These shifts are to lower binding energies and are consistent with the steepening of the top of the valence-band edge, with disorder, as observed in photoemission measurements. Finally, our results also account for the merging of the E_1 and the E_2 peaks of the imaginary part of the dielectric function ϵ_2, with disorder, as observed by spectroscopic ellipsometry and reflectivity measurements.

I. INTRODUCTION

Recent progress in the preparation of amorphous silicon (a-Si) (Refs. 1 and 2) has accelerated the search for a better understanding of the physics of group-IV amorphous semiconductors. It has been known experimentally for a long time that the basic tetrahedral co-ordination of group-IV atoms is retained in these materials apart from a small number of dangling bonds.[3]

In particular, measurements of the imaginary part of the dielectric function ϵ_2 of glow-discharge a-Si:H (Ref. 4) suggest the merging of the E_1 and E_2 peaks in c-Si. Also, the luminescence peak and optical gap from absorption measurements on a-Si:F:H are located at 1.2—1.3 and 1.7 eV, respectively. These values reflect possible connections to the corresponding indirect gaps, $\Gamma_{25'} \rightarrow X_1(\Delta_1)$ and $\Gamma_{25'} \rightarrow L_1$ of c-Si. Although the existence of a medium-range order for a a-Si has been established only for highly P- and As-doped a-Si:F:H (Ref. 5) and for a-Si:H under high rf power,[6] Phillips has put forth a topological model emphasizing medium-range order under strain.[7] Thus, a disorder model emphasizing distortions in the basic tetrahedral unit of c-Si may provide some quantitative understandings.

Although there have been many theoretical studies of the electronic structure of a-Si and a-Ge,[3,8—10] a study of the band structure of the normal crystalline phase under the influence of specific kinds of disorder has never been performed. The first attempts along this direction were by Ziman,[11] Kramer and Treusch,[12] and Cohen *et al.*[13] Their approximations, however, were rather simple and the disorder considered was not of a very specific nature. In the present study, therefore, we attempt to determine the effects of various kinds of *specific* quantitative disorder on the band structures of Si and Ge. In particular, we consider small distortions, including extensions and contractions of bond lengths, various bond-angle changes, and dihedral-angle variations in the normal crystalline phase of Si and Ge. The electronic states are modeled using a realistic tight-binding Hamiltonian including third-nearest-neighbor interactions. This Hamiltonian

gives reliable valence bands and low-lying conduction bands for c-Si and c-Ge. Disorder is introduced in a scheme reminiscent of the virtual crystal approximation[14] that is exact for bond-length distortions and approximate for bond-angle and dihedral-angle distortions.

The format of this paper is as follows: In Sec. II we describe the construction of our tight-binding Hamiltonian. In Sec. III we introduce a simple scheme based on (1) an exact transformation taking the Hamiltonian for the distorted structure to a diamondlike structure and (2) an approximation to the matrix elements of this Hamiltonian. In the framework of this scheme the effects of various small distortions on the band structures of c-Si and c-Ge at high symmetry points are determined. The results obtained are discussed in Sec. IV.

II. CONSTRUCTION OF THE TIGHT-BINDING HAMILTONIAN

There have been many band calculations for the diamond structure using the linear combination of atomic orbitals (LCAO) or tight-binding approach.[15] It has recently been pointed out that the inclusion of up to third-nearest-neighbor interactions in the LCAO Hamiltonian is indispensable for reliable band calculations of c-GaAs and c-Si.[16] In fact, omission of such interactions leads to unsatisfactory conduction-band energies and wave functions for c-Si and c-Ge.[13,17] Moreover, it is also known that one should, strictly speaking, also include d atomic orbitals (AO) into the LCAO basis in order to describe the conduction-band states of Si correctly.[18]

In the present treatment, we include the important interactions up to some third-nearest-neighbor atoms to obtain reliable band structures of c-Si and c-Ge, but omit d AO for the sake of simplicity. This is not a bad approximation for Ge since the energy level of $4d$ AO of Ge is considerably higher than that of $4p$ AO.[19] In order to pick up the important neighbor interactions, we use hybrid valence orbitals (VO) for the basis set. The VO employed here (Fig. 1) are sp^3 hybridized orbitals which simplify the selection of the most important second- and third-neighbor interactions that need to be considered. The selected interaction matrix elements are defined in Fig. 2. It is obvious that the third-nearest-neighbor interactions such as V_{10} and V_{11} will be more important than some of the second-nearest-neighbor ones owing to their distances and orientations. Thus the less important second-

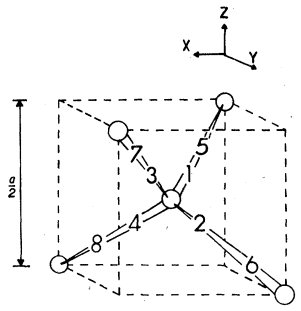

FIG. 1. Numbering of the eight VO in a unit cell.

neighbor interactions are discarded. The overlap integrals between any two different VO in the secular equations are assumed to be zero. This is equivalent to an assumption that the VO have been already orthogonalized through, e.g., the usual Löwdin's orthogonalization technique.[20] Closed-form expressions of the eigenvalues for Γ, X, and L points are obtained in a straightforward manner in terms of the interaction matrix elements V_n, which are treated as parameters. Those are given in the Appendix.

The V_n parameters are determined semiempirically so as to reproduce the numerical eigenvalues in good accordance with the standard experimental results for c-Si (Ref. 21) and c-Ge.[22] The values of the parameters used are given in column 2 of Table I. The calculated eigenvalues at Γ, X, and L points of c-Si and c-Ge are listed in the second

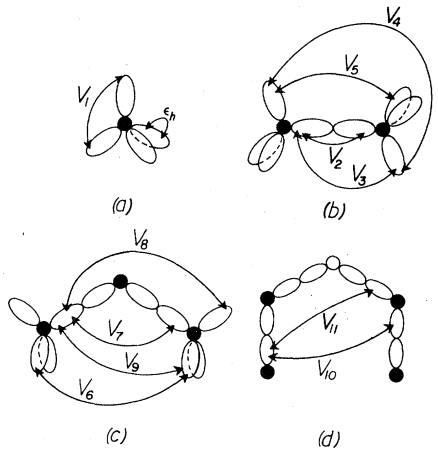

FIG. 2. Definitions of the interaction matrix elements between the VO located as (a) the one center, (b) the first-nearest neighbors, (c) the second-nearest neighbors, and (d) the third-nearest neighbors. Dark circles are atoms in the plane of the paper and a white one is that above the plane.

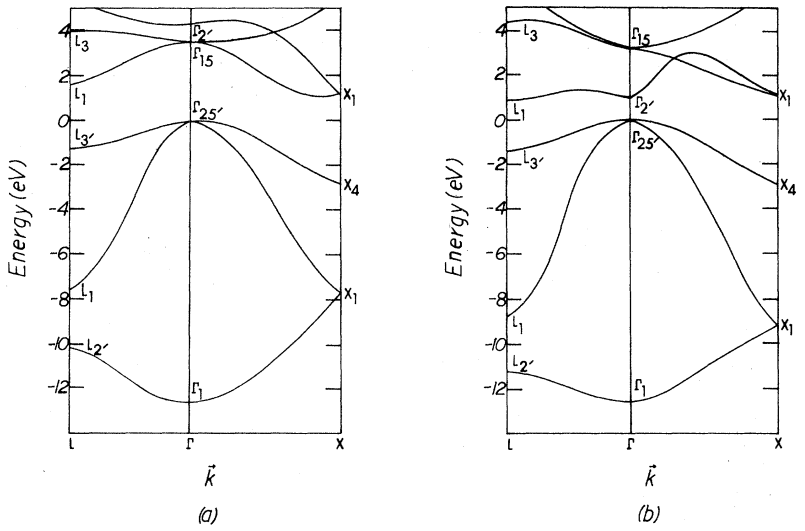

FIG. 3. Schematical drawing of the band structures of (a) c-Si and (b) c-Ge.

column of Tables II and III, respectively. Although the optimization of the eigenvalues has not been fully attempted, the overall features of the bands are satisfactory (Fig. 3) and offer a reasonable starting point for our analyses in the next section. It is also to be noted, from Table I, that the third-nearest-neighbor interaction such as V_{11} plays an important role as is expected.

TABLE I. Values of the parameters of the crystalline (V_n) and the distorted phases ($\tilde{V}_n$) for Si and Ge (in eV).

			Bond-length changes	
	$\tilde{V}_n$	Crystalline	Extensions	Contractions
Si	$\tilde{V}_1$	−1.145	−1.145	−1.145
	$\tilde{V}_2$	−4.014	−3.932	−4.099
	$\tilde{V}_3$	−0.445	−0.436	−0.454
	$\tilde{V}_4$	0.397	0.388	0.405
	$\tilde{V}_5$	−0.580	−0.568	−0.592
	$\tilde{V}_6$	0.027	0.026	0.027
	$\tilde{V}_7$	−0.704	−0.689	−0.719
	$\tilde{V}_8$	0.130	0.127	0.133
	$\tilde{V}_9$	0.095	0.093	0.097
	$\tilde{V}_{10}$	−0.089	−0.087	−0.091
	$\tilde{V}_{11}$	0.197	0.193	0.201
Ge	$\tilde{V}_1$	−1.072	−1.072	−1.072
	$\tilde{V}_2$	−4.390	−4.300	−4.482
	$\tilde{V}_3$	−0.401	−0.393	−0.409
	$\tilde{V}_4$	0.615	0.603	0.628
	$\tilde{V}_5$	−0.519	−0.508	−0.530
	$\tilde{V}_6$	0.049	0.048	0.050
	$\tilde{V}_7$	−1.260	−1.234	−1.287
	$\tilde{V}_8$	0.063	0.062	0.065
	$\tilde{V}_9$	0.119	0.117	0.122
	$\tilde{V}_{10}$	−0.061	−0.060	−0.062
	$\tilde{V}_{11}$	0.272	0.266	0.278

III. CALCULATIONS OF THE EFFECTS OF DISORDER

We should like to consider the effects of specific kinds of structural distortions on the electronic states of *c*-Si and *c*-Ge. Specifically, we will consider distortions consisting of (1) bond-length extensions, (2) bond-length contractions, (3) bond-angle changes with (a) compression with respect to a [111] axis, (b) extension to a [111] axis, (c) shearing to a [111] axis, and (d) compression to a [100] axis, and (4) dihedral-angle deviations. The bond-angle and dihedral-angle changes are illustrated in Fig. 4. All of these distortions are taken into account in the following manner.

We consider a weakly distorted structure such that there is a *simple* one-to-one correspondence between the atoms in this system and atoms in the diamond structure. If the Hamiltonian for the distorted structure of identical atoms is given by H_a, we can transform it to a new Hamiltonian $\tilde{H}_a$ which describes a system of nonidentical atoms placed on a perfect diamond structure. The relation between H_a and $\tilde{H}_a$ is given simply by

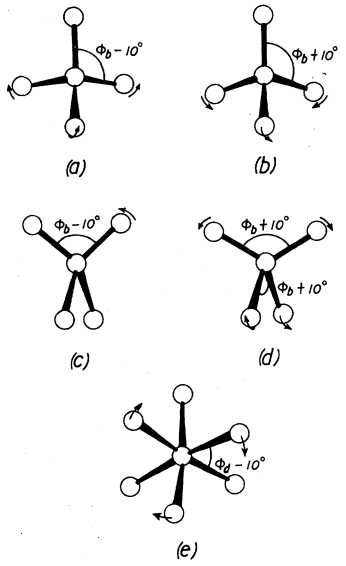

FIG. 4. The modes of the bond-angle changes ($a \sim d$) and the dihedral-angle deviations (e); (a) the compression with respect to a [111] axis, (b) the extension to a [111] axis, (c) the shearing to a [111] axis, and (d) the compression to a [100] axis. ϕ_b and ϕ_d are 109°28′ and 60°, respectively, of the normal crystalline phase.

TABLE I. *(Continued).*

Bond-angle changes				
[111] compression	[111] extension	[111] shearing	[100] compression	Dihedral-angle changes
−1.145	−1.145	−1.145	−1.145	−1.145
−3.937	−3.937	−3.989	−3.989	−4.014
−0.459	−0.459	−0.500	−0.450	−0.445
0.371	0.371	0.388	0.388	0.387
−0.566	−0.566	−0.575	−0.575	−0.575
0.028	0.028	0.027	0.028	0.049
−0.721	−0.724	−0.704	−0.703	−0.704
0.134	0.134	0.130	0.130	0.130
0.099	0.099	0.097	0.098	0.095
−0.092	−0.097	−0.090	−0.092	−0.079
0.205	0.214	0.198	0.207	0.201
−1.072	−1.072	−1.072	−1.072	−1.072
−4.302	−4.302	−4.361	−4.360	−4.390
−0.416	−0.416	−0.406	−0.406	−0.401
0.586	0.586	0.606	0.606	0.604
−0.503	−0.503	−0.513	−0.513	−0.513
0.050	0.050	0.049	0.049	0.091
−1.291	−1.297	−1.261	−1.260	−1.260
0.065	0.065	0.064	0.064	0.064
0.126	0.126	0.123	0.129	0.119
−0.062	−0.066	−0.062	−0.064	−0.047
0.282	0.295	0.274	0.285	0.277

TABLE II. Critical eigenvalues of Si and their deviations according to the distortions[a] (in eV).

Point	level	c-Si	Bond-length changes Extensions	Contractions
Γ	Γ_1	−12.50	+0.17	−0.18
	$\Gamma_{25'}$	0.00	+0.01	−0.01
	Γ_{15}	3.41	−0.06	+0.06
	$\Gamma_{2'}$	4.15	−0.17	+0.18
X	X_1	−7.69	+0.11	−0.11
	X_4	−2.90	+0.07	−0.07
	X_1	1.20	−0.05	+0.05
	X_3	5.32	−0.10	+0.10
L	$L_{2'}$	−10.23	+0.13	−0.14
	L_1	−7.50	+0.15	−0.16
	$L_{3'}$	−1.20	+0.03	−0.03
	L_1	1.46	−0.11	+0.11
	L_3	3.90	−0.07	+0.07
	$L_{2'}$	5.23	−0.11	+0.11

[a]The + and − signs stand for the ascent and descent from the eigenvalue positions of c-Si, respectively.

TABLE III. Critical eigenvalues of Ge and their deviations according to the distortions[a] (in eV).

Point	level	c-Ge	Bond-length changes Extensions	Contractions
Γ	Γ_1	−12.60	+0.17	−0.18
	$\Gamma_{25'}$	0.00	~0	~0
	$\Gamma_{2'}$	0.99	−0.11	+0.11
	Γ_{15}	3.23	−0.06	+0.07
X	X_1	−9.15	+0.15	−0.15
	X_4	−2.90	+0.06	−0.07
	X_1	1.26	−0.07	+0.07
	X_3	6.25	−0.13	+0.13
L	$L_{2'}$	−11.15	+0.16	−0.16
	L_1	−8.72	+0.18	−0.18
	$L_{3'}$	−1.40	+0.03	−0.03
	L_1	0.82	−0.10	+0.10
	L_3	4.30	−0.08	+0.09
	$L_{2'}$	5.95	−0.13	+0.14

[a]See the footnote of Table II.

TABLE II. *(Continued).*

Bond-angle changes				
[111] compression	[111] extension	[111] shearing	[100] compression	Dihedral-angle changes
+0.06	+0.07	+0.03	+0.09	+0.22
~0	−0.04	−0.01	−0.04	+0.15
+0.06	+0.12	+0.01	+0.03	+0.12
~0	−0.04	+0.03	~0	+0.05
~0	−0.01	~0	−0.01	−0.07
+0.20	+0.23	+0.06	+0.09	−0.04
−0.09	−0.08	−0.03	−0.01	−0.02
−0.16	−0.19	−0.05	−0.07	−0.05
−0.01	−0.02	~0	−0.01	−0.07
+0.11	+0.06	+0.05	+0.03	+0.22
+0.11	+0.12	+0.03	+0.03	−0.08
−0.02	−0.02	~0	+0.01	~0
−0.06	−0.07	−0.03	−0.03	−0.01
−0.17	−0.13	−0.05	−0.02	+0.04

TABLE III. *(Continued).*

Bond-angle changes				
[111] compression	[111] extension	[111] shearing	[100] compression	Dihedral-angle changes
+0.06	+0.10	+0.05	+0.18	+0.37
~0	−0.04	−0.02	−0.08	+0.29
−0.05	−0.12	+0.04	+0.06	+0.14
+0.05	+0.11	~0	+0.01	+0.23
−0.03	−0.06	~0	−0.04	−0.12
+0.25	+0.29	+0.08	+0.13	−0.08
−0.10	−0.08	−0.03	−0.04	−0.05
−0.15	−0.18	−0.05	−0.06	−0.09
−0.04	−0.06	~0	~0	−0.12
+0.12	+0.06	+0.06	+0.02	+0.33
+0.12	+0.14	+0.03	+0.03	−0.12
−0.01	+0.01	~0	+0.02	+0.01
−0.06	−0.06	−0.03	−0.04	−0.05
−0.19	−0.15	−0.06	−0.03	+0.13

$$\tilde{H}_a = \sum_i \sum_j \sum_\alpha \sum_\beta \langle h_\alpha(\vec{r}-\vec{r}_i)\,|\,H_a\,|\,h_\beta(\vec{r}-\vec{r}_j)\rangle\,|\,h_\alpha(\vec{r}-\vec{R}_i)\rangle\langle h_\beta(\vec{r}'-\vec{R}_j)\,|\ , \tag{1}$$

where h_α designates the αth VO ($\alpha = 1 \sim 4$) centered on a site, $\vec{r}_i$ locates the ith site in the distorted system, and $\vec{R}_i$ simply stands for the sum of the lattice site vector and the basis vector for the site i in the crystalline system. This $\tilde{H}_a$ is of a nonperiodic form, so we assume the site potential to be statistically periodic by averaging the matrix elements of $\tilde{H}_a$, that is, the interaction matrix elements are represented using an approximate Hamiltonian $\bar{H}_a$ by

$$\tilde{V}_n \equiv \langle h_\alpha(\vec{r}-\vec{r}_i)\,|\,\bar{H}_a\,|\,h_\beta(\vec{r}-\vec{r}_j)\rangle = \sum_{k=1}^{N} \frac{\langle h_\alpha(\vec{r}-\vec{R}_i-\vec{R}_k)\,|\,\tilde{H}_a\,|\,h_\beta(\vec{r}-\vec{R}_j-\vec{R}_k)\rangle}{N}\ . \tag{2}$$

Formally, there are infinite numbers of $\vec{R}_k$ in the system. It is to be noted that this procedure yields the exact results for the cases of the bond-length extensions and contractions, which cause a dilatation and a compression of the bulk crystal, respectively. For the cases of the bond-angle changes and the dihedral-angle deviations, the choice of $\vec{R}_k$ is assumed to be limited within a cluster involving up to the third-nearest-neighbor atoms concerned. This truncation method is reminiscent of the effective-crystal approximation employed by Kramer and Treusch.[12] Both method are in the framework of the virtual-crystal approximation which is valid for small distortions.[14]

The bond lengths are extended or contracted by 1.04% from their original lengths. These values are extracted from the relaxed continuous random tetrahedral network (CRTN) model of Steinhardt *et al.*[23] In the bond-angle changes and the dihedral-angle deviations, the fluctuations of the angles are assumed to be 10°.[24] With respect to these angle changes, the bond lengths are assumed to remain the same with those in the crystalline phase. The details of the calculations of the $\tilde{V}_n$'s in the distorted systems are relegated to the Appendix. The fluctuations of $\tilde{V}_n$'s thus obtained (Table I) result in the movements of the positions of the energy band of the crystalline structures. The complete results for the deviations in the critical eigenvalues and their band gaps due to the various distortions are listed in Tables II and III for Si and Ge, respectively, and in Table IV the features of which are discussed in the next section. It should be noted that this methodology is similar in spirit to the examination of ideal network structure for *a*-Si by Cohen *et al.*,[13] but provides more specific and quantitative information as shown later. Since we focus our attention on relatively small distortions, the topological disorder is not considered in the present study. Nevertheless, the exclusion of this factor still seems

TABLE IV. Changes of the band gaps of *c*-Si and *c*-Ge according to the distortions[a] (in eV).

			Bond-length changes	
		Crystalline	Extensions	Contractions
Si	$\Delta(\Gamma_{25'}\rightarrow\Gamma_{15})$	3.41	3.34(−0.07)	3.48(+0.07)
	$\Delta(\Gamma_{25'}\rightarrow X_1)$	1.20	1.14(−0.06)	1.26(+0.06)
	$\Delta(\Gamma_{25'}\rightarrow L_1)$	1.46	1.34(−0.12)	1.58(+0.12)
	$\Delta(X_4\rightarrow X_1)$	4.10	3.98(−0.12)	4.22(+0.12)
	$\Delta(L_{3'}\rightarrow L_1)$	2.66	2.52(−0.14)	2.80(+0.14)
	$\Delta(L_{3'}\rightarrow L_3)$	5.10	5.00(−0.10)	5.20(+0.10)
Ge	$\Delta(\Gamma_{25'}\rightarrow\Gamma_{2'})$	0.99	0.88(−0.11)	1.10(+0.11)
	$\Delta(\Gamma_{25'}\rightarrow X_1)$	1.26	1.19(−0.07)	1.33(+0.07)
	$\Delta(\Gamma_{25'}\rightarrow L_1)$	0.82	0.72(−0.10)	0.92(+0.10)
	$\Delta(X_4\rightarrow X_1)$	4.16	4.03(−0.13)	4.30(+0.14)
	$\Delta(L_{3'}\rightarrow L_1)$	2.22	2.09(−0.13)	2.35(+0.13)
	$\Delta(L_{3'}\rightarrow L_3)$	5.70	5.59(−0.11)	5.82(+0.12)

[a]The positive and the negative values in the parentheses stand for the blue shift and the red shift from the values of the crystalline band gaps, respectively, of Si and Ge.

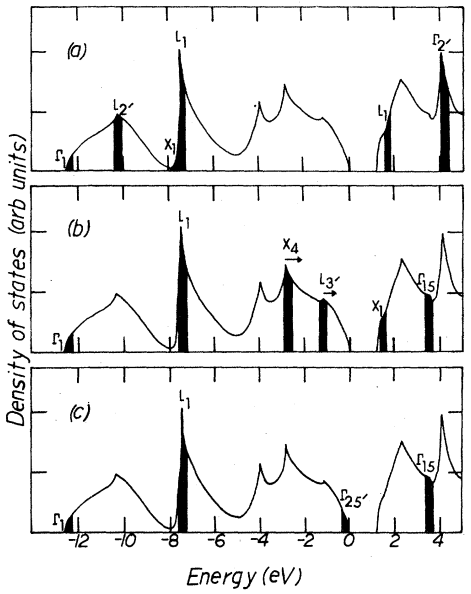

FIG. 5. Sketches of the DOS of c-Si and its mainly affected regions (black areas) under (a) the bond-length distortions, (b) the bond-angle distortions, and (c) the dihedral-angle deviations. The arrows in (b) indicate the directions of the movings of X_4 and $L_{3'}$ peaks to steepen the top of the valence band.

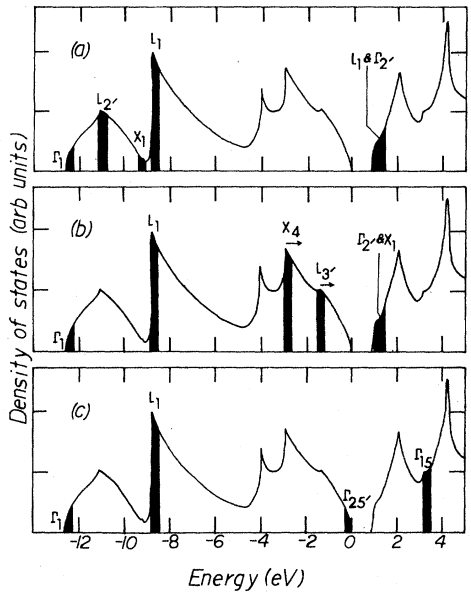

FIG. 6. Sketches of the DOS of c-Ge and its mainly affected regions. See the caption of Fig. 5.

to be plausible since it has been concluded that the rings, particularly the five-membered ones, in the CRTN models do not directly contribute to the band gap, the top portion of the valence band, and the valence-band width.[25,26]

IV. RESULTS AND DISCUSSION

From the results shown in Tables II, III, and IV, one can figure out the sensitive points of Γ, X, and L symmetries and the behavior of the band gaps due to each distortion. The regions of the density of states (DOS) mainly affected are sketched in Figs. 5

TABLE IV. *(Continued).*

Bond-angle changes				
[111] compression	[111] extension	[111] shearing	[100] compression	Dihedral-angle changes
3.47(+0.06)	3.57(+0.16)	3.43(+0.02)	3.48(+0.07)	3.38(−0.03)
1.11(−0.09)	1.16(−0.04)	1.18(−0.02)	1.23(+0.03)	1.03(−0.17)
1.44(−0.02)	1.48(+0.02)	1.47(+0.01)	1.51(+0.05)	1.31(−0.15)
3.81(−0.29)	3.79(−0.31)	4.01(−0.09)	4.00(−0.10)	4.12(+0.02)
2.53(−0.13)	2.52(−0.14)	2.63(−0.03)	2.64(−0.02)	2.74(+0.08)
4.93(−0.17)	4.91(−0.19)	5.04(−0.06)	5.04(−0.06)	5.17(+0.07)
0.94(−0.05)	0.91(−0.08)	1.05(+0.06)	1.13(+0.14)	0.84(−0.15)
1.16(−0.10)	1.22(−0.04)	1.25(−0.01)	1.30(+0.04)	0.92(−0.34)
0.81(−0.01)	0.87(+0.05)	0.84(+0.02)	0.92(+0.10)	0.54(−0.28)
3.81(−0.35)	3.79(−0.37)	4.05(−0.11)	3.99(−0.17)	4.19(+0.03)
2.09(−0.13)	2.09(−0.13)	2.19(−0.03)	2.21(−0.01)	2.35(+0.13)
5.52(−0.18)	5.50(−0.20)	5.64(−0.06)	5.63(−0.07)	5.77(+0.07)

and 6 for Si and Ge, respectively. It is seen that each distortion influences the DOS in a peculiar manner. We discuss these effects stepwise in Secs. IV A – IV C.

A. Bond-length changes

The bond-length extensions cause a rise of the points of the valence band and a lowering of those of the conduction band. This is to be expected from a decrease in the overlaps among the VO, namely the couple forming the bonds. The bond-length contractions give the opposite effects within a small range of the deviations.[27]

The sensitive points of the valence band to the bond-length changes are Γ_1, X_1, $L_{2'}$, and L_1 for both Si and Ge. We note that all of these points are *s*-like in character. The fluctuations in energy of these points would conceivably create localized states in the DOS near these regions as shown in Figs. 5 and 6. This is perhaps most likely in regions where the DOS is small. In the conduction band it is the L_1 and $\Gamma_{2'}$ points of Si and Ge that are most sensitive to the bond-length distortions. Therefore, the lower edge of the conduction band of Ge is affected more than that of Si. On the other hand, interestingly, $\Gamma_{25'}$ points of both Si and Ge are least sensitive among the other points.

All the band-gap changes (Table IV) show the red and the blue shifts according to the bond-length extensions and contractions, respectively, for both Si and Ge. Because of the insensitiveness of $\Gamma_{25'}$ points, the band gaps corresponding to direct transitions at X and L points ($X_4 \rightarrow X_1$ and $L_{3'} \rightarrow L_1$) are more strongly influenced than those corresponding to indirect transitions such as $\Gamma_{25'} \rightarrow X_1$ (therefore, assuming $\Gamma_{25'} \rightarrow \Delta_1$ min) in Si and $\Gamma_{25'} \rightarrow L_1$ in Ge. Hence, under the bond-length distortions, the deviation of the optical band gap is not large for both Si and Ge. The behavior of the direct band gaps ($X_4 \rightarrow X_1$ and $L_{3'} \rightarrow L_1$) is to be discussed in Sec. IV B in connection with the experimental results.

B. Bond-angle changes

The results from all the kinds of bond-angle changes considered in the present study show the same trends for points in the valence band. Since the shearing with respect to a [111] axis consists of the distortion of only one of the sp^3 bonds in each unit cell (Fig. 4), the fluctuations of the eigenvalues are smaller than those of other types of the bond-angle changes. It should be noted that, although the bond lengths are kept fixed to those of the normal crystalline phase, the second- and third-nearest-neighbor distances fluctuate inevitably as a consequence of the change of the bond angles.

All four kinds of the bond-angle distortions primarily cause the shifts of the *p*-like regions in the valence band. That is, the fluctuation of $L_{3'}$ takes place in a large amount under the compression and the extension with respect to a [111] axis, that of L_1 under the shearing to a [111] axis, and that of X_4 under all four kinds of the distortions for both Si and Ge. These indicate that the distortions of the directions of the sp^3 tetrahedral bonds cause the destabilization of the binding energies, leading to the steepening of the DOS at the top of the valence-band edge of both Si and Ge. These steepenings are consistent with the experimental information obtained from ultraviolet[28] and x-ray[29] photoemission measurements. The occurrence of the steepening of the higher valence-band edge has been also shown using the structural models for *a*-Si and *a*-Ge such as ST-12 (Ref. 30) and so on.[26] Joannopoulos has also reached the same conclusion by analyzing the Bethe-lattice model for Si in which the bond angles are intentionally fluctuated.[25]

Furthermore, the lower valence-band edge is affected by the compression with respect to a [100] axis for both Si and Ge. This type of compression tends to flatten out the distorted tetrahedron (Fig. 4) like a normal vibrational mode of E symmetry. It is interesting to point out that the destabilization occurs at the lowest *s*-like region accordingly as the tetrahedral coordination deforms into the planar coordination.

The fluctuations of the points of the conduction band are relatively small except those of Γ_{15} of Si and $\Gamma_{2'}$ of Ge due to the extension with respect to a [111] axis. These behaviors of Γ points will be interpreted by the fluctuations of the second- and third-neighbor interatomic distances which is mentioned above. The behaviors of the high-lying points such as X_3 or $L_{2'}$ of the conduction band are not discussed here since their positions in the crystalline phase are still somewhat too low in the framework of the tight-binding approach.

It is not practical to comment on the shift of the optical-absorption edge under these bond-angle distortions, since the indirect band gaps concerned with Si and Ge behave individually due to each distortion. On the other hand, typical deviation of the band gap for the transition of $X_4 \rightarrow X_1$ is seen for

all four kinds of the bond-angle distortions. This deviation is to be expected from the degradation of the [100] direction, namely, that of the long-range order, due to these distortions.

The spectroscopic ellipsometry for a-Si prepared by the laser annealing[31] and the reflectivity measurement[4] of glow-discharge a-Si:H have shown the imaginary part ϵ_2 of the dielectric function of these materials. According to them, it seems that the E_1 ($L_{3'} \rightarrow L_1$) and the E_2 ($X_4 \rightarrow X_1$) peaks gradually merge into one around the E_1 peak of c-Si, as the normal crystalline phase changes into the amorphous state. The same kind of observations have been obtained for a-Si and a-Ge prepared by sputtering.[28,32–35] This tendency is clearly reproduced by any kinds of bond-angle distortions in the present result, showing that the band-gap corresponding to the $X_4 \rightarrow X_1$ transition causes a red shift moving much faster than that corresponding to the $L_{3'} \rightarrow L_1$ transition. The red shifts of these band gaps are also seen in the case of the bond-length extensions. By this distortion, however, no typical merging of the E_1 and the E_2 peaks may be expected because of the same rate of the shifts of these peaks. It is also interesting to point out that the E_2 peak may be smeared out or even be put out at some stage of the bond-angle distortions because of the *fragility* of this peak resulting from the [100] direction as described above.

C. Dihedral-angle deviations

Generally speaking, uniform dihedral-angle deviations cause a considerably large change of the atomic arrangement in the bulk network of Si and Ge, even if the deviation angle is small. Therefore, the interpretation of the result in this case should be made with certain reservations. We consider only the most striking features in our discussion.

All Γ points of the valence band and the conduction band, except $\Gamma_{2'}$, and L_1 of the former band, seem to be sensitive to the dihedral-angle deviations. These may cause the localization near both the lower and the higher valence-band edges of Si and Ge. The indirect gaps due to the transitions from $\Gamma_{25'}$ are significantly redshifted, leading to the lowering of the optical-absorption edge of both Si and Ge. Another consequence of the dihedral-angle distortions is the tendency of causing the $L_{3'}$ and X_4 points to merge into a single-bump structure in the p-like region of the valence band.

V. CONCLUDING REMARKS

We have studied various kinds of quantitative disorders on the band structures of Si and Ge to model the electronic structures of a-Si and a-Ge. The results indicate that each distortion causes the shifts of the band of c-Si and c-Ge in an individual manner, and do apply to spectroscopic observations being characteristic of a-Si and a-Ge. Moreover, they suggest regions in the DOS where localization might occur. There are three major features in the present study:

(1) The bond-length distortions influence mainly the lower part of the valence band and may cause localization around Γ_1 and X_1 regions where the DOS is small. In Ge the bottom of the conduction band is also affected.

(2) All of the bond-angle changes are responsible for the steepening of the top of the valence-band edge, as observed for a-Si and a-Ge. In addition, these distortions may create localization near Γ_1.

(3) The observed merging of the E_1 and the E_2 peaks of ϵ_2 function is accounted for by any of the bond-angle distortions.

Moreover, the dihedral-angle deviations may give rise to gap states and also cause a bump structure of DOS in the p-like region of the valence band.

Finally, we like to point out that the extension of the present scheme of the calculation, such as the average T-matrix approximation, will also become a good tool, as a first-order approximation, for the probe of modeled electronic structures for a-Si or a-Ge, including two or more elements like hydrogen, fluorine, and so on, on account of its considerably simple algorithm.

ACKNOWLEDGMENTS

The interest of S. R. Ovshinsky in this work is greatly appreciated. This work was performed under partial support by ARCO Ventures Company, a division of Atlantic Richfield.

APPENDIX

The closed forms of the eigenvalues of the tight-binding Hamiltonian in Sec. II are obtained as follows for Γ, X, and L points in the order of increasing the energy:

$$\Gamma_1 = \epsilon_h + 3V_1 + V_2 + 6V_3 + 3V_4 + 6V_5 + 6V_6 + 3V_7 + 6V_8 + 12V_9 + 6V_{10} + 6V_{11} ,$$

$$\Gamma_{25'} = \epsilon_h - V_1 + V_2 - 2V_3 + 3V_4 - 2V_5 + 6V_6 - V_7 + 6V_8 - 4V_9 + 6V_{10} - 2V_{11} \text{ (triply degenerate)} ,$$

$$\Gamma_{15} = \epsilon_h - V_1 - V_2 + 2V_3 - 3V_4 + 2V_5 + 6V_6 - V_7 + 6V_8 - 4V_9 - 6V_{10} + 2V_{11} \text{ (triply degenerate)} ,$$

$$\Gamma_{2'} = \epsilon_h + 3V_1 - V_2 - 6V_3 - 3V_4 - 6V_5 + 6V_6 + 3V_7 + 6V_8 + 12V_9 - 6V_{10} - 6V_{11} ,$$

$$X_1 = \epsilon_h + V_1 - 2V_6 + V_7 - 2V_8 - 4V_9 - [(-V_2 - 2V_3 + V_4 + 2V_5 + 2V_{10} + 2V_{11})^2 + 4(V_1 - V_7)^2]^{1/2} \text{ (doubly degenerate)} ,$$

$$X_4 = \epsilon_h - V_1 + V_2 - 2V_3 - V_4 + 2V_5 - 2V_6 - V_7 - 2V_8 + 4V_9 - 2V_{10} + 2V_{11} \text{ (doubly degenerate)} ,$$

$$X_1 = \epsilon_h + V_1 - 2V_6 + V_7 - 2V_8 - 4V_9 + [(-V_2 - 2V_3 + V_4 + 2V_5 + 2V_{10} + 2V_{11})^2 + 4(V_1 - V_7)^2]^{1/2} \text{ (doubly degenerate)} ,$$

$$X_3 = \epsilon_h - V_1 - V_2 + 2V_3 + V_4 - 2V_5 - 2V_6 - V_7 - 2V_8 + 4V_9 + 2V_{10} - 2V_{11} \text{ (doubly degenerate)} , \tag{A1}$$

$$L_{2'} = \epsilon_h + V_1 + 2V_3 + 2V_4 + 2V_6 + V_7 - 2V_8 - 4V_{10} - \tfrac{1}{2}[(-2V_1 - 2V_2 - 4V_3 + 2V_4 + 8V_6 - 2V_7 - 8V_8 - 4V_{10})^2 + 12(V_1 + 2V_5 - V_7 - 2V_{11})^2]^{1/2} ,$$

$$L_1 = \epsilon_h + V_1 - 2V_3 - 2V_4 + 2V_6 + V_7 - 2V_8 + 4V_{10} - \tfrac{1}{2}[(2V_1 - 2V_2 - 4V_3 + 2V_4 - 8V_6 + 2V_7 + 8V_8 - 4V_{10})^2 + 12(V_1 - 2V_5 - V_7 + 2V_{11})^2]^{1/2} ,$$

$$L_{3'} = \epsilon_h - V_1 + V_2 - 2V_3 + V_4 - 2V_6 - V_7 + 2V_8 - 2V_{10} \text{ (doubly degenerate)} ,$$

$$L_1 = \epsilon_h + V_1 - 2V_3 - 2V_4 + 2V_6 + V_7 - 2V_8 + 4V_{10} + \tfrac{1}{2}[(2V_1 - 2V_2 - 4V_3 + 2V_4 - 8V_6 + 2V_7 + 8V_8 - 4V_{10})^2 + 12(V_1 - 2V_5 - V_7 + 2V_{11})^2]^{1/2} ,$$

$$L_3 = \epsilon_h - V_1 - V_2 + 2V_3 - V_4 - 2V_6 - V_7 + 2V_8 + 2V_{10} \text{ (doubly degenerate)} ,$$

$$L_{2'} = \epsilon_h + V_1 + 2V_3 + 2V_4 + 2V_6 + V_7 - 2V_8 - 4V_{10} + \tfrac{1}{2}[(-2V_1 - 2V_2 - 4V_3 + 2V_4 + 8V_6 - 2V_7 - 8V_8 - 4V_{10})^2 + 12(V_1 + 2V_5 - V_7 - 2V_{11})^2]^{1/2} .$$

In the above expressions ϵ_h signifies the orbital energy of a hybrid valence orbital (Fig. 2), which can be treated as a constant.

Next, we outline how to numerate the interaction matrix elements $\tilde{V}_n$ for the distorted system using Eq. (2). Since it is too space consuming to describe here about every $\tilde{V}_n$ for all cases of the distortions, we restrict ourselves only to visualize the way of the estimations of $\tilde{V}_n$'s, taking $\tilde{V}_9$ in the case of the compression with respect to a [100] axis as an example.

At first, it is convenient to decompose the V_n's for the crystalline phase into the AO interaction terms as follows:

$$V_1 = \tfrac{1}{4}(\epsilon_s - \epsilon_p) ,$$

$$V_2 = \tfrac{1}{4}[A_{ss}(r_1) + 2\sqrt{3}A_{sp}(r_1) + 3A_{pp\sigma}(r_1)] ,$$

$$V_3 = \tfrac{1}{4}\left[A_{ss}(r_1) + \frac{2\sqrt{3}}{3}A_{sp}(r_1) - A_{pp\sigma}(r_1)\right] ,$$

$$V_4 = \tfrac{1}{4}\left[A_{ss}(r_1) - \frac{2\sqrt{3}}{3}A_{sp}(r_1) + \frac{1}{3}A_{pp\sigma}(r_1) - \frac{8}{3}A_{pp\pi}(r_1)\right] ,$$

$$V_5 = \frac{1}{4}\left[A_{ss}(r_1) - \frac{2\sqrt{3}}{3}A_{sp}(r_1) + \frac{1}{3}A_{pp\sigma}(r_1) + \frac{4}{3}A_{pp\pi}(r_1)\right] ,$$

$$V_6 = \frac{1}{4}[A_{ss}(r_2) + 3A_{pp\pi}(r_2)] ,$$

$$V_7 = \frac{1}{4}[A_{ss}(r_2) + 2\sqrt{2}A_{sp}(r_2) + 2A_{pp\sigma}(r_2) + A_{pp\pi}(r_2)] ,$$

$$V_8 = \frac{1}{4}[A_{ss}(r_2) - 2A_{pp\sigma}(r_2) + A_{pp\pi}(r_2)] ,$$

$$V_9 = \frac{1}{4}[A_{ss}(r_2) + \sqrt{2}A_{sp}(r_2) - A_{pp\pi}(r_2)] ,$$

$$V_{10} = \frac{1}{4}\left[A_{ss}(r_3) + \frac{6\sqrt{11}}{11}A_{sp}(r_3) + \frac{9}{11}A_{pp\sigma}(r_3) - \frac{24}{11}A_{pp\pi}(r_3)\right] ,$$

$$V_{11} = \frac{1}{4}\left[A_{ss}(r_3) + \frac{6\sqrt{11}}{11}A_{sp}(r_3) + \frac{9}{11}A_{pp\sigma}(r_3) + \frac{20}{11}A_{pp\pi}(r_3)\right] . \quad \text{(A2)}$$

Here ϵ_s, ϵ_p, and $A_{\mu\nu}(r_i)$ are, respectively, the orbital energies of the $3s$ ($4s$ for Ge) AO, the $3p$ ($4p$ for Ge) AO, and the interaction matrix elements between AO χ_μ and χ_ν. The centers of these χ's are separated by r_i. Explicitly, they become as follows:

$$\epsilon_s = \langle \chi_s | H | \chi_s \rangle ,$$
$$\epsilon_p = \langle \chi_p | H | \chi_p \rangle , \quad \text{(A3)}$$
$$A_{\mu\nu}(r_i) = \langle \chi_\mu | H | \chi_\nu \rangle ,$$

where H is the Hamiltonian. The four kinds of the $A_{\mu\nu}(r_i)$ interactions are shown in Fig. 7, and r_i, r_2, and r_3 are the distances up to the first-, second-, and third-nearest-neighbor atoms, respectively. The expressions for $V_1 \sim V_5$ in Eq. (A2) are identical to those given by Pantelides and Harrison.[36] We do not have to mind the explicit values of ϵ_s and ϵ_p here because V_1 does not change its value for any kinds of disorder on account of its nature as the one-center interaction. Therefore, all of the values for $A_{\mu\nu}(r_i)$ should be assigned from Eq. (A2) using the values of V_n's in the second column of Table I. The $\{A_{\mu\nu}(r_3)\}$ is obtained by adding two third-neighbor interactions other than V_{10} and V_{11}, the values of which are assumed to be zero.

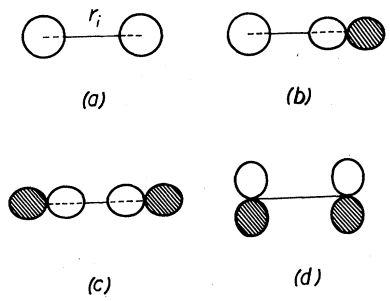

FIG. 7. Notations of $A_{\mu\nu}(r_i)$ interactions. (a) $A_{ss}(r_i)$, (b) $A_{sp}(r_i)$, (c) $A_{pp\sigma}(r_i)$, and (d) $A_{pp\pi}(r_i)$.

For $\tilde{V}_9$ in the case of the compression with respect to a [100] axis, three different kinds of terms, V_9^*, V_9^{**}, and V_9^{***}, are required as the numerator in Eq. (2), which originate from the three different kinds of spatial configurations of the VO concerned as illustrated in Fig. 8. These terms are given by the following expressions:

$$V_9^* = \frac{1}{4}[A_{ss}(r_2^*) + \sqrt{2}A_{sp}(r_2^*) - A_{pp\pi}(r_2^*)] ,$$

$$V_9^{**} = \frac{1}{4}[A_{ss}(r_2^{**}) + 1.272\,968A_{sp}(r_2^{**}) - 0.189\,776A_{pp\sigma}(r_2^{**}) - 1.189\,776A_{pp\pi}(r_2^{**})] , \quad \text{(A4)}$$

$$V_9^{***} = \frac{1}{4}[A_{ss}(r_2^{**}) + 1.542\,580A_{sp}(r_2^{**}) + 0.189\,776A_{pp\sigma}(r_2^{**}) - 0.810\,224A_{pp\pi}(r_2^{**})] .$$

In the above expressions r_2^* and r_2^{**} are $1.058r_2$ and $0.970r_2$, respectively, in the present case of the distortion. The deviated values of $A_{\mu\nu}(r)$ in the

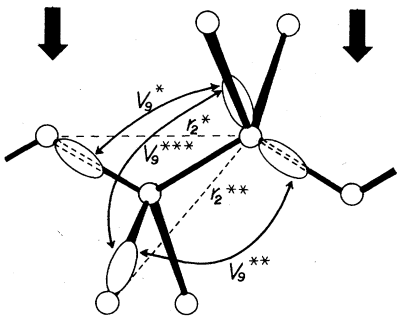

FIG. 8. Definitions of the interactions, V_9^*, V_9^{**}, and V_9^{***} under the compression with respect to a [100] axis (indicated by arrows). Note that each VO lobe is not on the bonding direction because of the distortion.

neighborhood of r_1, r_2, and r_3 are calculated using the d^{-2} scaling.[37] This scaling for $\{A_{\mu\nu}(r)\}$ is also employed for the calculations of $\tilde{V}_n$'s in the cases of the bond-length changes.

Now $\tilde{V}_9$ is given by

$$\tilde{V}_9 = \frac{V_9^* + V_9^{**} + V_9^{***}}{3} , \qquad \text{(A5)}$$

by the consideration of the equal weight of V_9^*, V_9^{**}, and V_9^{***} in the present case. It is to be noted that this weight in the average depends on specific $\tilde{V}_n$ for each distorted system. All the other $\tilde{V}_n$'s are to be estimated in a similar fashion described here.

[1]W. E. Spear and P. G. LeComber, J. Non-Cryst. Solids 8—10, 727 (1972); A. Madan, P. G. LeComber, and W. E. Spear, *ibid.* 20, 239 (1976).

[2]S. R. Ovshinsky and A. Madan, Nature 276, 482 (1978); A. Madan, S. R. Ovshinsky, and E. Benn, Philos. Mag. B. 40, 259 (1979); A. Madan, S. R. Ovshinsky, and W. Czubatyj, J. Electron. Mater. 9, 385 (1980); A. Madan, J. McGill, W. Czubatyj, J. Yang, and S. R. Ovshinsky, App. Phys. Lett. 37, 826 (1980).

[3]N. F. Mott and E. A. Davis, *Electronic Processes in Non-Crystalline Materials,* 2nd ed. (Clarendon, Oxford, 1979), Chap. 7.

[4]G. Weiser, D. Ewald, and M. Milleville, J. Non-Cryst. Solids 35-36, 447 (1980).

[5]R. Tsu, M. Izu, S. R. Ovshinsky, and F. H. Pollack, Solid State Commun. 36, 817 (1980); R. Tsu, M. Izu, V. Cannella, S. R. Ovshinsky, G-J. Jan, and F. H. Pollak, in *Proceedings of the Fifteenth International Conference on Physics of Semiconductors, Kyoto, 1980* [J. Phys. Soc. Jpn. 49, Suppl. A, 1249 (1980)].

[6]A. Matsuda, S. Yamasaki, K. Nakagawa, H. Okushi, K. Tanaka, S. Iizima, M. Matsumura, and H. Yamamoto, Jpn. J. Appl. Phys. 19, L305 (1980); T. Hamasaki, H. Kurata, M. Hirose, and Y. Osaka, Appl. Phys. Lett. 37, 1084 (1980).

[7]J. C. Phillips, J. Non-Cryst. Solids 35-36, 1157 (1980).

[8]J. D. Joannopoulos and M. L. Cohen, Solid State Phys. 31, 71 (1976).

[9]*Amorphous Semiconductors,* edited by M. H. Brodsky (Springer, Berlin, 1979).

[10]*Amorphous and Liquid Semiconductors,* Proceedings of the Eighth International Conference on Amorphous and Liquid Semiconductors, Boston, Massachusetts, 1979, edited by W. Paul and M. Kastner (North-Holland, Amsterdam, 1980).

[11]J. Ziman, J. Phys. C 4, 3129 (1971).

[12]B. Kramer and J. Truesch, in *Proceedings of the Twelfth International Conference on Physics of Semiconductors, Stuttgart, 1974* (Teubner, Stuttgart, 1974), p. 1061.

[13]M. H. Cohen, J. Singh, and F. Yonezawa, J. Non-Cryst. Solids 35-36, 55 (1980); J. Singh, Phys. Rev. B 23, 4156 (1981).

[14]See, for example, E. J. Elliott, J. A. Krumhansl, and P. L. Leath, Rev. Mod. Phys. 46, 465 (1974); E. N. Economou, *Green's Functions in Quantum Physics* (Springer, Berlin, 1979).

[15]See, for example, W. A. Harrison, *Electronic Structures and the Properties of Solids* (Freeman, San Francisco, 1980) and references therein.

[16]Y. Wang and J. D. Joannopoulos, J. Vac. Sci. Technol. 17, 997 (1980); D. A. Papaconstantopoulos and E. N. Economou, Phys. Rev. B 22, 2903 (1980).

[17]K. C. Pandey and J. C. Phillips, Phys. Rev. B 13, 750 (1976).

[18]E. O. Kane, Phys. Rev. B 13, 3478 (1976); S. G. Louie, *ibid.* 22, 1933 (1980).

[19]See, for example, G. Höjer and S. Meza, Acta Chem. Scand. 26, 3723 (1972).

[20]P.-O. Löwdin, J. Chem. Phys. 18, 365 (1950).

[21]See the references in J. R. Chelikowski and M. L. Cohen, Phys. Rev. B 10, 5095 (1974).

[22]See the references in K. C. Pandey and J. C. Phillips, Phys. Rev. B 9, 1552 (1974).

[23]P. Steinhardt, R. Alben, and D. Weaire, J. Non-Cryst. Solids 15, 199 (1974).

[24]See, for example, Ref. 8 and references therein.

[25]J. D. Joannopoulos, Phys. Rev. B 16, 2764 (1977).

[26]W. Y. Ching, C. C. Lin, and L. Guttman, Phys. Rev. B 16, 5488 (1977).

[27]Explicit electron repulsion interactions should be taken into account in the discussion of the case of an extreme bond-length contractions.

[28]T. M. Donovan and W. E. Spicer, Phys. Rev. Lett. 21, 1572 (1968).

[29]L. Ley, S. Kowalczyk, R. Pollak, and D. A. Shirley, Phys. Rev. Lett. 29, 1088 (1972).

[30]J. D. Joannopoulos and M. L. Cohen, Phys. Rev. B 7, 2644 (1973).

[31]D. E. Aspnes, G. K. Celler, J. M. Poate, G. A. Rozgonyi, and T. T. Sheng, in *Proceedings of the Symposium on Laser and Electron Beam Processing of Electronic Materials,* edited by C. L. Anderson, G. K. Celler, and G. A. Rozgonyi (The Electrochemical Society, Princeton, 1980), p. 414.

[32]D. Beaglehole and M. Zanetowa, J. Non-Cryst. Solids 4, 272 (1970).

[33]T. M. Donovan, W. E. Spicer, J. M. Bennett, and E. J. Ashley, Phys. Rev. B 2, 397 (1970).

[34]D. T. Pierce and W. E. Spicer, Phys. Rev. B 5, 3017 (1972).

[35]J. Stuke and G. Zimmerer, Phys. Status Solidi B 49, 513 (1972).

[36]S. T. Pantelides and W. A. Harrison, Phys. Rev. B 11, 3006 (1975).

[37]See p. 149 of Ref. 15 and references therein.